The heterogeneity and electro-mechanical characteristics of coal at the micro-and nanoscale

Weixiang Wang
University of Science and Technology Beijing, University of Alberta

Dazhao Song
University of Science and Technology Beijing

Xueqiu He
University of Science and Technology Beijing, University of Wollongong, hexq@uow.edu.au

Xianfeng Liu
Chongqing University

Zhenlei Li
University of Science And Technology Beijing

See next page for additional authors

Recommended Citation

The heterogeneity and electro-mechanical characteristics of coal at the micro- and nanoscale

Abstract

With regard to the mechanism of electromagnetic radiation (EMR) excited by deformation and failure of coal and rock, the present study employed the optical microscope, digital microhardness tester and atomic force microscopy (AFM) to measure surface morphology, surface microhardness and electro-mechanical characteristics, including elastic modulus and surface potential of coal. The results show that micro-mineral composition and micro-mechanical properties of coal are clearly heterogeneous. The elastic modulus values measured are 62.3 MPa-4.0 GPa and the surface potential values tested are 21.2-166.2 mV. The proportion distributions of the two parameters mentioned follow the normal distribution, which indicates the electro-mechanical characteristics of coal are clearly inhomogeneous at the micro-and nanoscales. Finally, the effects of the inhomogeneous elastic modulus and surface potential on the EMR from the microscopic perspective were analyzed. In this experiment, the change of the micro-elastic modulus and the existence of the surface potential on the coal surface were directly observed. The findings reveal the mechanism of EMR induced by deformation and failure of coal and rock.

Disciplines

Engineering | Science and Technology Studies

Publication Details

Authors

Weixiang Wang, Dazhao Song, Xueqiu He, Xianfeng Liu, Zhenlei Li, and Xianghui Tian

The heterogeneity and electro-mechanical characteristics of coal at the micro- and nanoscale

Weixiang Wang [1,2], Dazhao Song[1,*], Xueqiu He[1,3], Xianfeng Liu[4], Zhenlei Li[1] and Xianghui Tian[1]

[1] School of Civil and Resources Engineering, University of Science and Technology Beijing, 30 Xueyuan Road, Haidian District, Beijing 100083, China

[2] Department of Chemical and Materials Engineering, University of Alberta, Edmonton, Alberta T6G 1H9, Canada

[3] School of Civil, Mining and Environmental Engineering, University of Wollongong, Wollongong, NSW 2522, Australia

[4] State Key Laboratory for Coal Mine Disaster Dynamics and Control, Chongqing University, 174 Shazheng Street, Shapingba District, Chongqing 400044, China

*Corresponding author: Dazhao Song. E-mail: song.dz@163.com

Abstract

With regard to the mechanism of electromagnetic radiation (EMR) excited by deformation and failure of coal and rock, the present study employed the optical microscope, digital microhardness tester and atomic force microscopy (AFM) to measure surface morphology, surface microhardness and electro-mechanical characteristics, including elastic modulus and surface potential of coal. The results show that micro-mineral composition and micro-mechanical properties of coal are clearly heterogeneous. The elastic modulus values measured are 62.3 MPa–4.0 GPa and the surface potential values tested are 21.2–166.2 mV. The proportion distributions of the two parameters mentioned follow the normal distribution, which indicates the electro-mechanical characteristics of coal are clearly inhomogeneous at the micro- and nanoscales. Finally, the effects of the inhomogeneous elastic modulus and surface potential on the EMR from the microscopic perspective were analyzed. In this experiment, the change of the micro-elastic modulus and the existence of the surface potential on the coal surface were directly observed. The findings reveal the mechanism of EMR induced by deformation and failure of coal and rock.

Keywords: electromagnetic radiation of coal and rock, AFM, elastic modulus, surface potential, heterogeneity

1. Introduction

In mines, coal and rock dynamic disasters (such as rock burst, coal and gas outburst, etc.) frequently occur that seriously threaten the safe development of mines. With an increase of mining depth, coal and rock dynamic disasters become more serious. Many engineering practices and laboratory experiments have confirmed that the deformation and failure of coal and rock could induce EMR (Frid 1997; Dou *et al.* 2005; Frid & Vozoff 2005; Wang *et al.* 2012; Li *et al.* 2017;

Qiu *et al.* 2018; Song *et al.* 2018). An accurate early warning technology for coal and rock dynamic disasters can improve mining safety. Coal and rock EMR technology has been proved to be a scientific and useful early warning technology by a large number of engineering practices, and many successful cases have been observed (Park *et al.* 1993; O'Keefe & Thiel 1995; Rabinovitch *et al.* 2007; He *et al.* 2010, 2012; Mastrogiannis *et al.* 2015; Song *et al.* 2016, 2017; Gade *et al.* 2017). However, the mechanism of EMR generated by

deformation and failure of coal and rock is still unclear at present. Many explanations have been offered, such as the piezoelectric effect, friction lifting, flow potential, electron hole migration and polarization induced by stress (Nitsan 1977; Enomoto *et al.* 1993; Guo & Liu 1995; Wang & He 2000; Qiu *et al.* 2017; He *et al.* 2019). But most of these explanations are based on experiments at the macro-level or hypotheses, and no consensus has been reached yet. Moreover, experimental research at the micro- and nanoscales has not been carried out in this field.

Coal is a heterogeneous natural combustible organic rock and has apparent heterogeneity because of its formation conditions, mineral composition, cementing material and various geological structures of occurrence, as well as many weak connections of different strengths in it. Failure of coal and rock is the result of large numbers of internal micro-destructions interconnecting with each other and breaking under stress along the direction where the strength is relatively weak (He *et al.* 2003). Many macro–micro-experimental results show that the surface potential of coal and rock caused by deformation and failure is a macro-physical phenomenon where coal and rock produce free charges in the process of deformation and failure (Li *et al.* 2009; He *et al.* 2013). According to the mechanism of free charge generation, there is a specific connection between free charge generation and micro-damage of coal and rock. Micro-damage of coal and rock is closely related to the micro-mechanical properties and the load state of micro-elements (Li *et al.* 2012). However, the electro-mechanical properties of coal and rock at the micro- and nanoscales have not been studied in detail yet.

Research at the micro- and nanoscale relies on very sophisticated testing methods. Atomic force microscopy (AFM), as an instrument with atomic-level precision in the field of material science, has been widely used in the research into electro-mechanical properties of solid materials at the micro- and nanoscales. Bruening & Cohen (2005) analyzed the roughness and hardness of macerals in coal using the quantitative function of AFM. Collins *et al.* (2014) studied the relationship between local structure, chemical composition and mechanical properties of bituminous coal by the confocal micro-Raman imager and the atomic force acoustic microscope. Liu *et al.* (2017) used a peak-force quantitative nano-mechanical (PF–QNM) atomic force microscope to measure the surface morphology, adhesion, modulus and deformation of oil sands in atmospheric conditions, to distinguish the adsorbed bitumen on the surface of the particle and determine its existing state. Li & Zeng (2014) obtained the nanoscale mechanical properties of abalone shells using a contact resonance force microscope (CR–FM). Adamcik *et al.* (2012) determined the elastic modulus and other mechanical properties of starch fibers by PF–QNM. Wang *et al.* (2014) used AFM to study the thickness and modulus distri-

bution of a polymer blend interface. Results showed accurate and intuitive data that are close to their macro-modulus. Trtik *et al.* (2012) studied the local elastic modulus of hardened cement paste by AFM with peak-force tapping mode, and found that the quantitative mapping of the local elastic modulus can discriminate different phases in the cement paste microstructure, which cannot be distinguished from the corresponding back-scattered electron images.

Huang *et al.* (2012a, 2012b) measured the microstructure and charge distribution of quartz sand using electrostatic force microscopy with a phase imaging mode. Yan *et al.* (2011) tested the surface charge distribution of silicate by AFM and confirmed that the silicate surface has a certain number of negative charges. Gao *et al.* (2016) studied the surface charge anisotropy of minerals and found that surface charge distribution is influenced by test environment. Guo & Yu (2017) obtained the average surface potential of kaolin and montmorillonite to be –40.9 and –62.71 mV, respectively. Yin & Drelich (2008) tested the interaction curves between the micro-surface of volcanic rocks and the probe by AFM, and one- and two-dimensional images of the surface potential of volcanic rocks were calculated using the DLVO theory. Kumar *et al.* (2016) observed the surface charge distribution of kaolinite nanoparticles using a dynamic atomic force microscope.

The results and conclusions above provide useful references for studying the electro-mechanical properties of coal and rock at the micro- and nanoscale. In this study, the primary focus was on the properties of micro-mechanics and electricity of coal. First, we studied the heterogeneity of material components and electro-mechanical characteristics of coal. After this, the reasons from the microscopic perspective for inhomogeneous failure and the generation of surface potential of coal were explored. Finally, their influence on the EMR excited by deformation and failure of coal was analyzed so as to give an insight into the research on the mechanism of EMR on the micro-basis. The micro-mechanical and electrical characteristics of rock will be conducted in future research.

2. Experiment

2.1. Sample preparation

AFM requires a very smooth test surface, so it is necessary to polish coal samples. The coal lumps were cut into thin pieces at a size of about 10 × 10 × 5 mm, and then these thin pieces were inlaid into cylinders using a XQ-2B inlaying machine to facilitate polishing and prevent the pieces from breaking. Next, the surfaces of the samples were polished to make sure the surface roughness was less than 100 nm (Yao *et al.* 2011) and both sides of the cylinder were smooth and parallel by employing the YMP-1 polishing machine.
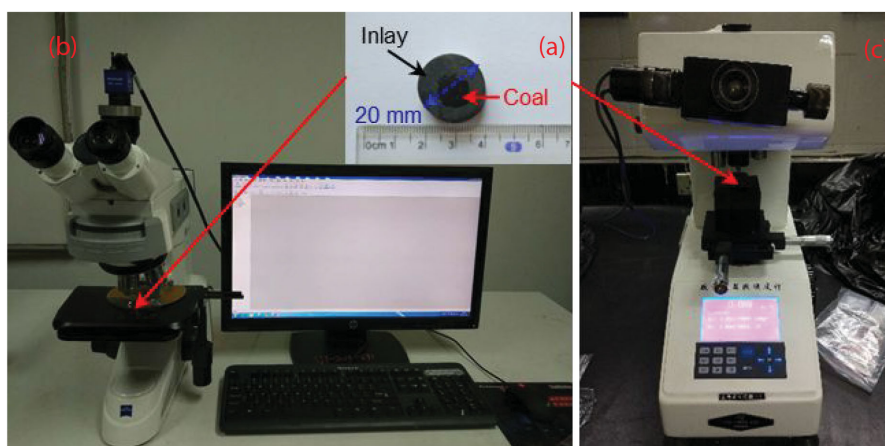
Figure 1. (a) Prepared coal sample, (b) optical microscope and (c) digital microhardness tester.

Finally, the coal samples were dried and sealed in order to prevent the adsorption of the impurities on the surface from affecting subsequent tests. A prepared coal sample is shown in figure 1a.

2.2. Optical measurement

(1) The prepared coal samples were put on the sample stage of the ZEISS Axiocam 105 Color optical microscope, as shown in figure 1b, to observe and photograph the surface morphologies.

(2) Then the HXD-1000TM digital microhardness tester, as shown in figure 1c, was used with a load of 200 gf (about 1.96 N) and holding for 10 s on the typical areas to qualitatively test the surface mechanical properties and mark the test areas for AFM measurement. The interval between the markers was about 100 μm, and the line spacing had to be appropriately adjusted. All of the markers formed a 4×4 array.

2.3. AFM measurement

The Dimension Icon AFM produced by the Bruker Company was used in this experiment. It chiefly consists of six components: a probe, a laser device that provides light, a piezoelectric scanner that performs grating scanning and Z-axis positioning, a micro-cantilever deflection detection device for force-separation feedback, a photoelectric detection feedback system for receiving optical feedback signals and a data collection and image processing system. The detailed schematic is shown in figure 2 (Christopher *et al.* 2012; Du *et al.* 2015). We selected the PF–QNM and the Kelvin probe force microscope (KPFM) to test the electro-mechanical properties of the marked areas on the coal surface.

2.3.1. Principle of PF–QNM. The PF–QNM mode is a new imaging mode in AFM that can quantitatively characterize
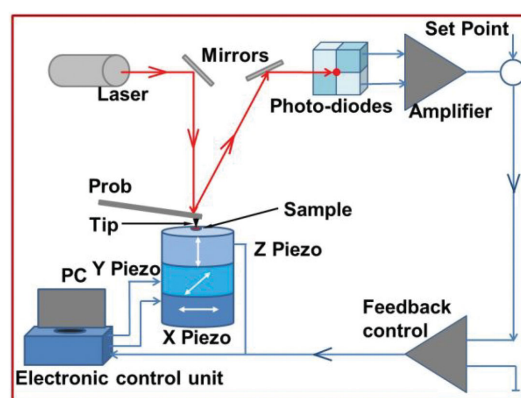

Figure 2. Schematic diagram of AFM.

the mechanical properties of materials at the nanoscale. The imaging principle is to apply a sine wave (the typical value of the frequency is ~0.5–2 kHz) with a driving frequency far below the resonance frequency of the AFM tip to the Z-direction of a scanning tube so that the probe can be intermittently exposed to the sample surface for a short time. At the time of scanning, the force curve is made at each contact point, and the constant peak force is used as the imaging feedback signal. Detailed information about the interaction between the probe tip and the sample on each contact point can then be obtained. After calibrating the elastic constant, the radius of curvature and the sensitivity of the probe with the standard method, the mechanical information distribution of the sample can be measured (Young *et al.* 2011; Dokukin & Sokolov 2012; Clark *et al.* 2013; Fernández *et al.* 2014). The typical force–separation curve obtained during AFM imaging by PF–QNM is shown in figure 3, while the abscissa is the distance between the probe tip and the sample, the ordinate represents the force between the probe tip and the sample. The Engage curve in figure 3 shows the relationship between the force and distance as the tip approaches to the sample surface, while the Withdraw curve indicates the
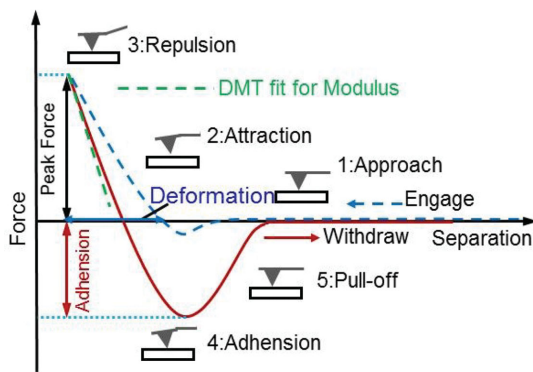
Figure 3. Schematic diagram of the PF-QNM technique.

relationship when the tip leaves the sample surface. To avoid the influence of the plastic deformation of the sample in the Engage curve, the Withdraw curve is used to obtain the elastic deformation of the sample. On the basis of the relationship between elastic deformation and force, the elastic modulus can be calculated using the Derjaguin–Muller–Toporov fit model and the calculation formula is as follows:

$$F - F_{\text{adh}} = \frac{4}{3} E^* \sqrt{R \cdot d} \qquad (1)$$

where F is the load exerted by AFM, F_{adh} is the adhesion force between the probe tip and the sample, R is the tip radius, d is the elastic deformation of the sample and E^* is the reduced elastic modulus. Then the elastic modulus of sample can be calculated by

$$\frac{1}{E^*} = \frac{1 - v_s^2}{E_s} + \frac{1 - v_t^2}{E_t} \qquad (2)$$

where v_s and v_t are the Poisson's ratios of the sample and probe, respectively, and E_s and E_t are the elastic moduli of the sample and probe, respectively (Tsukruk *et al.* 2003; Butt *et al.* 2005).

2.3.2. Principle of KPFM. KPFM, which combines the atomic force microscopy with the Kelvin probe, is a technology used to measure the surface potential of materials (Liscio *et al.* 2008). When the probe tip contacts the sample, the charge transfer will occur on the contact surface due to the difference of work function between the two, thus forming a stable contact potential difference. For the probe and the sample, if there is a potential difference between them, an alternating electric field force will make the probe cantilever vibrate. If the potential difference is zero, there is no electric field force and the amplitude of the cantilever is also zero. In the measurement process, a DC compensation voltage is usually applied between the probe and the sample. By adjusting the voltage, the system eliminates the primary contact potential difference between them, which makes the amplitude of the cantilever zero. Then the surface poten-

tial distribution of sample is measured (Ashcroft & Mermin 1976).

In this experiment, we fixed and connected the marked coal samples with the AFM sample stage by conductive adhesives. The probe used was SCM-PIT-V2, with a spring constant k of 2.8 N m^{-1}, resonant frequency f_0 of 60 kHz and tip radius of 20 nm. The scan range was 5×5 μm, the scan frequency 1 Hz, the lift height of the probe 200 nm and image resolution 256×256. All the measurements were carried out in a stable atmospheric environment (a temperature of 20°C and humidity at 30%). Nanoscope Analyses software was used for image acquisition and data processing.

3. Experiment results

3.1. Optical characterization of coal heterogeneity

Figure 4 shows the micro-surface morphologies characterization of coal from the Wudong coal mine (WD, gas-fat coal) in Xinjiang, the Xin-Zhouyao coal mine (XZY, 1/3 coking) in the Shanxi Province, the Malan coal mine (ML, coking coal) in the Shanxi Province and the Da-Shucun coal mine (DSC, anthracite) in the Hebei Province, respectively, obtained by an optical microscope. There are clear differences between the portions inside and outside the green line frame on the coal samples in figure 4. According to the various colors, the heterogeneity of the material composition at the microscale can be seen directly, which is mainly due to the differences in forming materials, forming conditions, mineral composition, cementing materials and so on.

Considering a large number of observation results on different coal samples obtained by the optical microscope, it can be found that this phenomenon is widespread. In this study, we took XZY coal samples as examples for detailed study. In figure 5, ignoring the scratches made during polishing, we can see that the colors on the micro-surface of coal sample are complex and there are many blocky and gray-white areas. The difference between these colors proves the heterogeneity of the coal composition. In addition, it can be clearly seen that there is a grayish strip region (the portion between the long green dashed lines) that divides the surface into three regions; namely, region I, II and III. Examining the array of the markers in these three regions, the marker sharpness of each row markers is more and more distinct, and the depth increases along the direction of the red arrow, which indicates the difference in the hardness and the inhomogeneity of the mechanical properties of the coal sample. In order to further quantitatively study the micro-mechanical properties of coal samples and explore their micro-electrical properties, three 5×5 μm test areas were selected at random in regions I, II and III, and then measured by AFM, respectively.
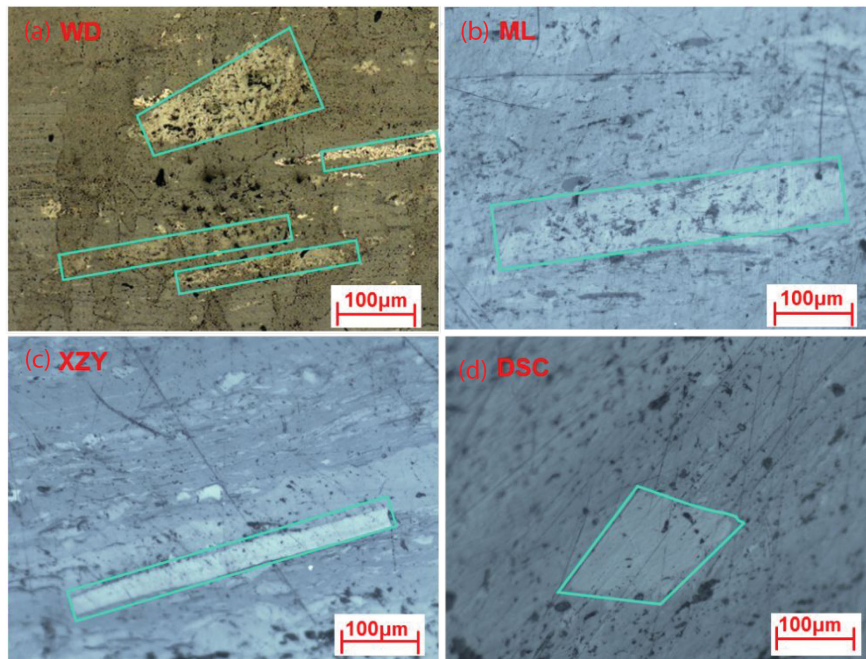
Figure 4. Micro-surface morphologies characterization of different coal samples obtained by the optical microscope.
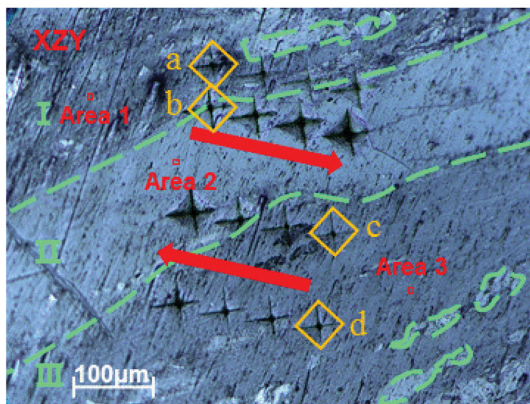

Figure 5. The morphology and marking image of a XZY coal sample.

3.2. The micro-mechanical properties of coal

Only one representative test area from each of regions I, II and III was examined in this study, denoted as Areas 1, 2 and 3, respectively (as shown in figure 5). Figure 6 illustrates the distribution of the elastic modulus of the three test areas. It can be seen that the elastic modulus values at the different points in the same test area are not the same, and elastic modulus values in different test areas also show a clear difference. The minimum modulus measured is 62.3 MPa and the maximum is 4 GPa. The proportion distributions of elastic modulus values and fitting curves in Areas 1–3 are shown in figure 7. It was found that the proportion distribution in each test area follows a clear normal distribution and the R^2 values of fitting curves are all more than 0.939. The elastic modu-

lus values of Areas 1 and 3 have wide ranges, which are 131.6 MPa–4.0 GPa and 62.3 MPa–1.1 GPa, respectively, and it was noted that the mechanical properties of Areas 1 and 3 were inhomogeneous. In contrast, the small range of elastic modulus distribution (219.3–522.1 MPa) in Area 2 showed more uniform mechanical properties than that in Areas 1 and 3.

The average and standard deviation of the elastic modulus of each of the three test areas in regions I, II and III in figure 5 are displayed in figure 8. It can then be concluded that average values of elastic modulus in regions I, II and III are 1.06, 0.34 and 0.7 GPa, respectively. The changes in the average and standard deviation have a positive consistency. The region with a large average elastic modulus also has a greater standard deviation, which indicates that the data in this region are more discrete and the inhomogeneity of this region is more distinct. It can be speculated that the material in region II is more homogeneous than that in regions I and III, and the difference of the mechanical properties of the micro-elements in region II is smaller. As shown in figures 6 and 7, as far as a single test area is concerned, the mechanical properties of coal sample in the nanoscale are inhomogeneous (the interval of each two adjacent points is about 19.5 nm). Taking the average value of elastic modulus in each test area as the characteristic value of the mechanical properties of this area, and according to figure 8, we can see that the mechanical properties of coal samples in the microscale also show inhomogeneity. According to figure 5, it also can be found that the mechanical properties of coal samples decrease first and then increase from regions I to III, and the interface of regions I and II, II and III can be taken as a relatively weak connection,
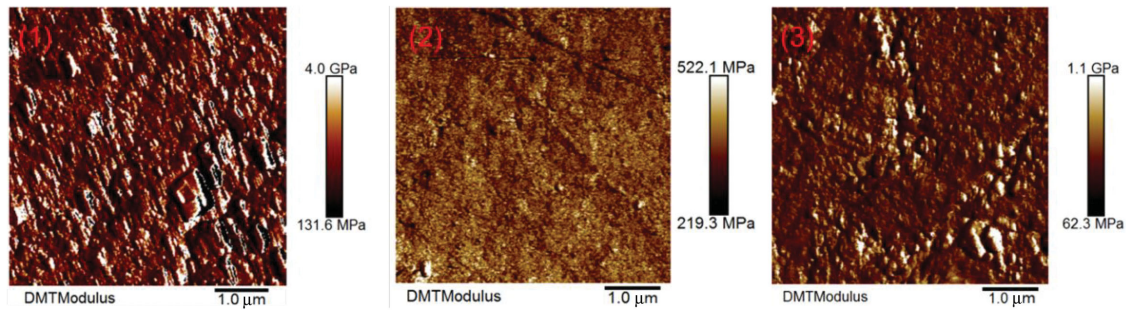
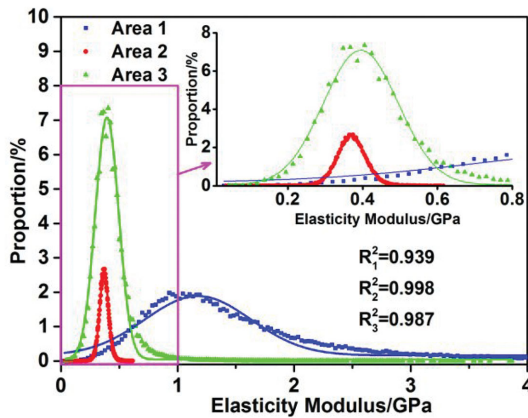**Figure 6.** Elastic modulus distributions of Areas 1–3.

Figure 7. Proportion distributions of elastic modulus and fitting curves in Areas 1–3.
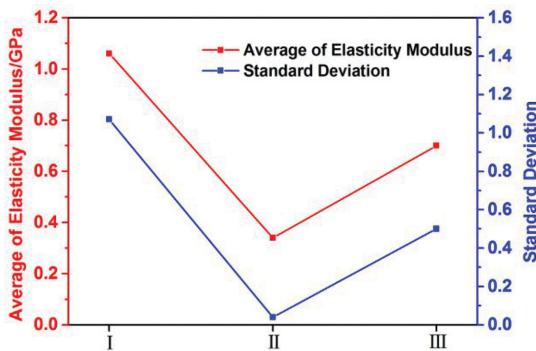

Figure 8. The average and standard deviation of elastic modulus of each three test areas in regions I–III.

which is often the breakthrough point of a macro fracture. In short, this test describes the inhomogeneity of the mechanical properties of coal samples quantitatively.

3.3. Micro-electrical characteristics of coal

Figure 9 shows the micro-surface morphologies and the surface potential distributions of Areas 1–3. It can be seen that the surface potential distribution is less correlated with the micro-surface morphology in this experiment, which is

mainly because the probe uses a two-scan method when measuring the surface potential. The first step is the Main Scan, and the surface morphology of the sample is obtained by the tapping mode. The second step is the Interleave Scan: the probe is lifted to a certain height, and an AC voltage V_{AC} sin ωt is applied to the probe. According to the morphology information obtained from the Main Scan, the system keeps the vertical distance between the probe and the sample constant and then measures the surface potential of sample. The whole process is shown in figure 10. Therefore, the measured values of surface potential are mainly related to the surface material and its physical and chemical structures and properties.

In figure 9d–e, the values of the bright yellow areas or points are large, and the values of the dark yellow areas or points are small. The bright areas (where the green frame is marked in the picture) are interlaced with the dark areas, and the bright points and the dark points alternate. Compared to figure 9d and f, there is no distinct bright or dark yellow area in figure 9e, and the surface potential distribution in figure 9e is relatively homogeneous. The surface potential values of Areas 1–3 measured are 21.2–122.0, 41.6–166.2 and 40.8–148.8 mV, respectively. The surface potential values of the coal sample on the microscale are not the same in the same test area and show distinct differences.

Figure 11 illustrates the proportion distributions of surface potential in Areas 1–3 and fitted curves. It can be observed that the proportion distributions of surface potential in Areas 1–3 also show the characteristics of a normal distribution with R^2 values all above 0.992. Figure 12 shows the average and standard deviation of the surface potential of each three test areas in regions I, II and III in figure 5. In figure 12, it can be seen that the average values of surface potential of each three test areas in regions I, II and III are 58.37, 119.35 and 76.35 mV, respectively. The standard deviation of surface potential in region II is smaller than that in regions I and III, which indicates that the discreteness of region II is smaller. Similarly, as shown in figures 9 and 11, the surface potential of the coal sample has obvious inhomogeneity at the nanoscale for each test area (the interval of each two adjacent points is about 19.5 nm). Taking the average value of the surface
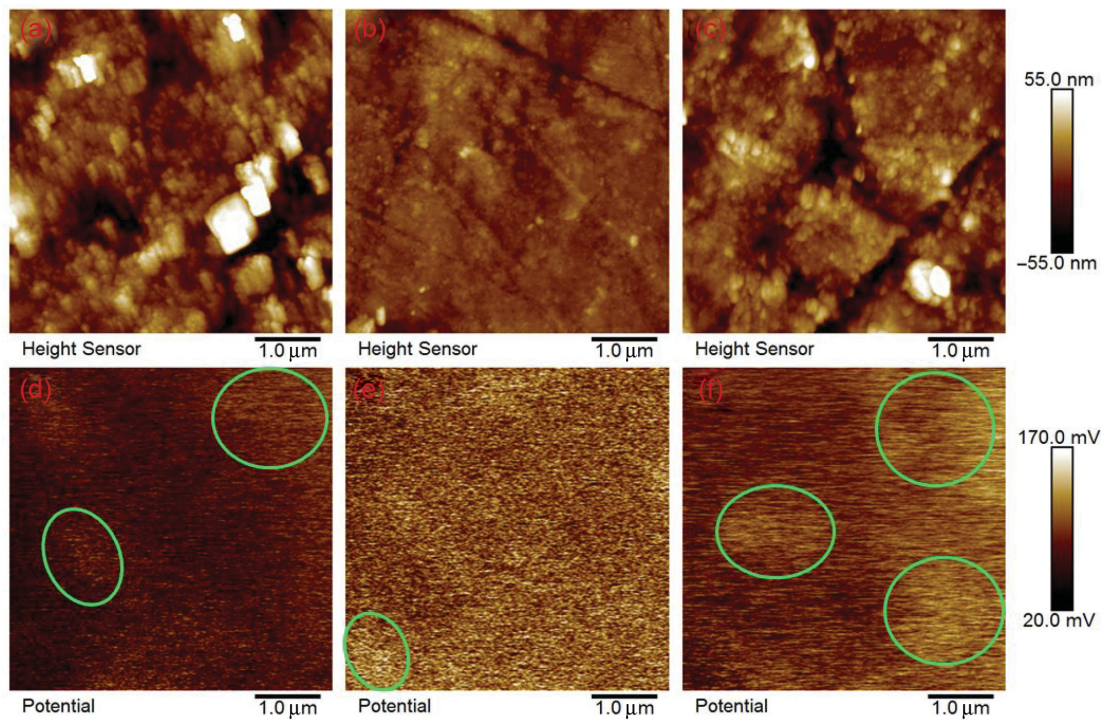
Figure 9. The surface morphologies a,b,c and surface potential distributions d,e,f of Area 1–3.
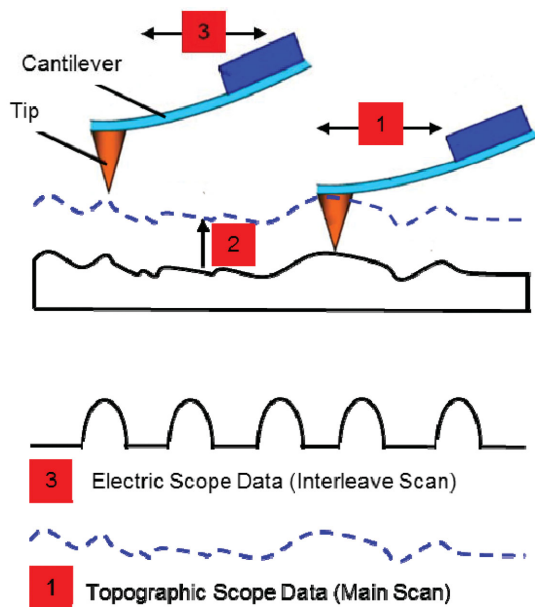

Figure 10. Schematic of the KPFM imaging process. The first step, the Main Scan, measuring the surface morphology; the second step, the probe is lifted to a certain height; in the third step, Interleave Scan, to measure the surface potential distribution.

Figure 11. Proportion distributions of surface potential and fitting curves in Areas 1–3.
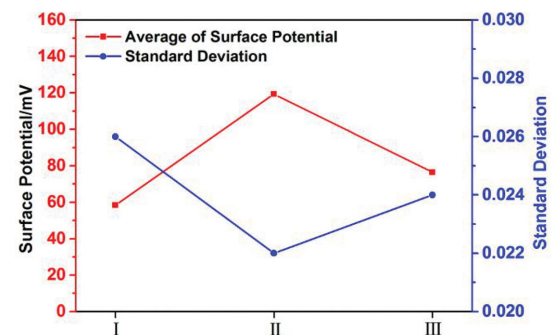
Figure 12. The average and standard deviation of surface potential of each three test areas in regions I–III.

potential in each test area as the characteristic value of the electrical properties of this area, and combining with figure 12, it can be seen that the surface potential of coal sample has clear inhomogeneity at the microscale.
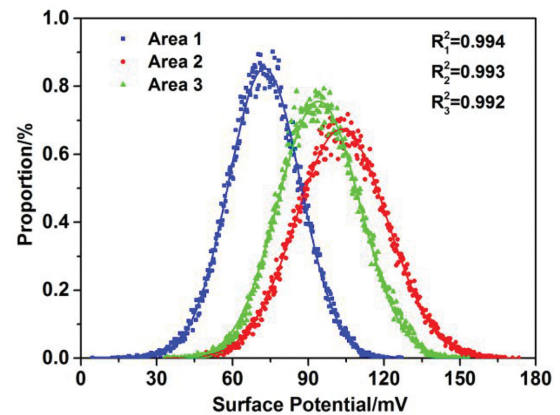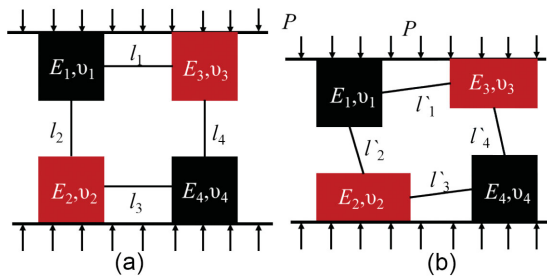
Figure 13. Schematic diagram of micro-deformation process of inhomogeneous coal mass.

4. Discussion

4.1. The discreteness of the micro-elastic modulus and its influence on micro-fracture

In this study, the micro-elastic modulus of coal samples has been quantitatively tested by AFM with values ranging from 62.3 MPa to 4.0 GPa, presenting noticeable differences and discrete distributions. This is because pores, fissures, dislocations, grain boundaries, multiphase medium and the size effect have a significant impact on the elastic modulus of coal at the microscale (Nie *et al.* 2015; Liu & Nie 2016). Furthermore, coal is mostly grain-aggregated, which can be seen even with the naked eye. Boundaries between grains also have a significant influence on the strength of coal. When the tip of the AFM probe falls on the inherent damage point or region of coal samples, the micro-elastic modulus values tested are smaller. When it falls on the backbone of coal samples, the micro-elastic modulus values are larger. Even if there is no apparent defect in coal, for most crystalline interfaces, the elastic modulus values of the same mineral grains are different due to the different orientations of mineral grains. In addition, the chemical bond is an important factor in determining the fracture resistance and crack propagation resistance. The various chemical bond types that make up the coal macromolecular structures also affect the micro-elastic modulus of coal.

It is assumed that the coal at each test point in the experiment is a micro-element. When the coal mass is loaded and the tensile strain generated on micro-elements exceeds its ultimate tensile strain, the interface between the strong and the weak micro-elements in the local area will be broken, which can be illustrated by a simple model as follows (Wang *et al.* 2009).

Suppose that the model consists of four elastic blocks that are glued together natively, as shown in figure 13a, where

$$E_1 = E_4 > E_2 = E_3, \upsilon_1 = \upsilon_4 < \upsilon_2 = \upsilon_3 \quad (3)$$

When axial stress is applied to the model, the model after deformation is shown in figure 13b. It can be seen that due to the difference of the elastic modulus E, l_1 and l_3 are stretched,

so $l'_1 > l_1$, $l'_3 > l_3$. Due to the difference of Poisson's ratio υ, the stretching of l_2 and l_4 is caused, so $l'_2 > l_2$, $l'_4 > l_4$. For coal, Poisson's ratio is less than 0.5, so the longitudinal deformation is larger than the lateral deformation under uniaxial compression, then equation (4) exists.

$$\frac{l'_1 - l_1}{l_1} = \frac{l'_3 - l_3}{l_3} > \frac{l'_2 - l_2}{l_2} = \frac{l'_4 - l_4}{l_4} \quad (4)$$

According to the ultimate tensile strain criterion, l'_1 and l'_3 will be fractured first, and the result of failure approximates the generation of longitudinal cracks. That is, due to the difference of elastic modulus, longitudinal shear tensile strain is caused and transverse shear tensile strain is caused by the difference of Poisson's ratio. As the final result, longitudinal shear cracks are created and micro-fractures are caused by the load. The heterogeneity of coal (such as the inhomogeneous elastic modulus, etc.) causes micro-fractures to penetrate each other in a relatively weaker direction under continuous load, resulting in inhomogeneous rupture of the coal mass.

4.2. The causes of surface potential generation and inhomogeneous distribution

There is a large number of crystal structures inside coal and it is well known from the theory of fracture mechanics that when the local stress of the crystal is equal to the theoretical breaking strength (Yu & Feng 1997), namely $\sigma = \sqrt{E\gamma/b}$, the local chemical bonds will be broken, forming micro-cracks. Here, σ is the local stress of the crystal, E is the elastic modulus, γ is the surface energy density of the crystal and b is the lattice spacing. Combining the results obtained in the experiments, we can conclude that due to the inhomogeneity of the micro-elastic modulus E, the theoretical fracture strength of the crystal in coal is inhomogeneous, so the coal will generate an inhomogeneous fracture due to inhomogeneous deformation when loaded. According to previous research results (Anderson 2005), the mode of crack propagation can be divided into three basic types: opening mode, sliding mode and tearing mode. No matter which mode of crack propagation occurs, the tip structures of the cracks will be destroyed. The macromolecular structures of the coal are separated and the chemical bonds are broken as well. Some of the chemical bonds become dangling bonds, and different charges are generated on the newly formed crack walls. Sliding, friction and so on appear on both sides of the micro-cracks, which can cause chemical bonds to break and generate more free charges that then form the potential on the micro-surface (Lv *et al.* 2013). This process is schematically shown in figure 14.

It is generally believed that coal macromolecules are formed by connecting polycondensation rings with a variety
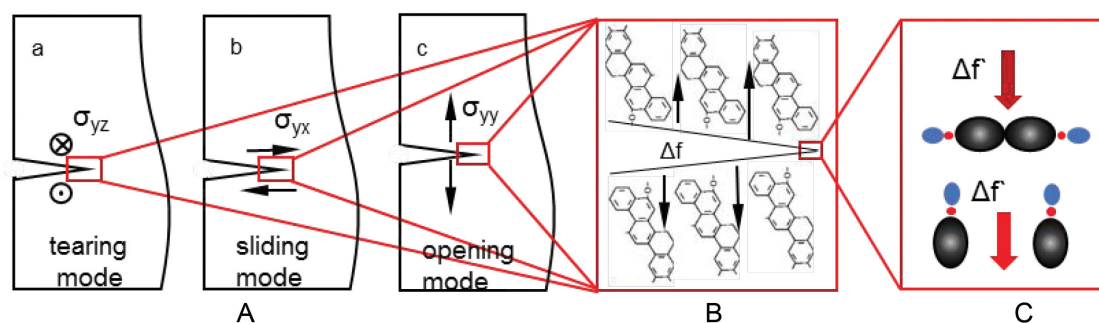
Figure 14. Schematic diagram of the types of micro-crack generation (A), the separation of coal macromolecules (B) and chemical bond breaking (C).

of atomic groups surrounding and hydrogenated aromatic condensed rings (collectively known as aromatic nuclei or basic structural units) through a variety of bridge bonds, such as methylene ($-CH_2-$, $-CH_2-CH_2-$, $-CH_2-CH_2-CH_2-$ etc.), oxygen bonds ($-O-$, $-CH_2-O-$ etc.) and sulfur bonds ($-S-$, $-S-S-$, $-CH_2-S-$ etc.) (Bodzek & Marzec 1981; Potgieter-Vermaak *et al.* 2011; He *et al.* 2017; Liu *et al.* 2019). The micro-cracks make different bridge bonds break into dangling chemical bonds that exhibit different electrical properties and charge quantities. Moreover, various functional groups of O, N, S and other impurity atoms are also contained in the organic structure of coal (Solum *et al.* 1997; Miura *et al.* 2001), and the electrical properties of different functional groups are also different (Garner-O'Neale *et al.* 2003). The non-chemical bonds between the coal macromolecules are very rich, exceeding the covalent bonds. The coal breaks along the macromolecular boundary and bonds broken in the fracture process are dominated by non-chemical bonds, followed by covalent bonds. These non-chemical bonds are destroyed, as well as covalent bonds, and also exhibit different electrical properties and charge quantities. In addition, the electrical dipoles presented on the coal surface will also show certain electrical properties. Together, these reasons are behind the inhomogeneous distribution of surface potential of coal samples at the micro- and nanoscale.

The analysis above can further explain the viewpoint on the mechanism of EMR of coal and rock proposed by Wang & He (2000), He *et al.* (2003) and Li *et al.* (2012); namely, the inhomogeneous deformation of the heterogeneous coal and rock mass produced by the load causes charges and makes charges migrate. As a large number of charges accumulate on the surface of coal samples, inhomogeneous surface potential is developed. Rabinovitch *et al.* (1998) proved that when the crack propagates forward, the atomic bonds at the tip of cracks will be broken, causing the atomic equilibrium state on both sides of the atomic bonds to break, thus inducing atomic perturbation. It is this atomic perturbation occurring with the crack propagation that excites the rock fractures and EMR.
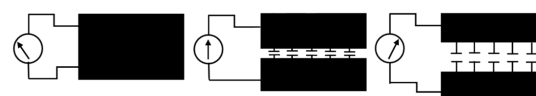

Figure 15. A crack expands in a material forming the two plates of a capacitor. The capacitor is charged or discharged by residual charges on the newly created surfaces during the oscillation of the crack.

4.3. The influence of micro-surface potential caused by fractures on EMR

Ogawa *et al.* (1985) proposed a capacitor model as a source of EMR generation based on crack propagation. It is believed that the properties of the charged particles on both sides of the expanded structural surfaces formed when the rock is broken are exactly opposite, and thus a capacitor formed is continuously charged and discharged, as shown in figure 15. At the same time, the EMR is generated. Based on this capacitor model, O'Keefe & Thiel (1995) proved the feasibility of the charge separation model as the source of EMR induced by the fracture of brittle materials. The currents flowing around the tip of the crack were then calculated according to an analytical expression and a finite-difference method.

In this study, the occurrence and propagation of micro-cracks in coal will produce charges and then cause surface potential. Assuming that each micro-crack is tiny and the surface potential is evenly distributed on the two surfaces of the crack, uniform electric field intensity can be calculated using the uniform electric field calculation formula $E = U/d$. According to the data tested here, $U = 100$ mV is selected. It is assumed that the distance between the two surfaces of the micro-cracks has been 1, 10 and 100 nm during the propagation, and the electric field intensity can reach 10^8, 10^7 and 10^6 V m^{-1}, respectively. It can be presumed that in the propagation process of micro-cracks, large and varied electric field intensity can be produced. According to the principle of electromagnetic dynamics (He *et al.* 2003), in the field source space with free charge, the changing electric field and magnetic field can be generated to induce EMR and propagate outward, as long as the free electrons move under certain
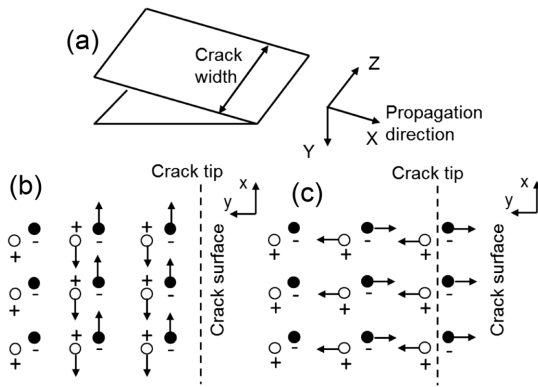
Figure 16. (a) Schematic diagram of crack propagation; (b) and (c) schematics of an 'optical surface wave' at the crack surface at a specific time (a similar wave propagates on the other surface). The crack surface is in the *x–z* plane, and the crack moves in the *x*-direction. The charge separation is oscillatory, so the dipole directions are reversed at a later time.

Figure 17. Schematic diagram of crack expansion in coal.

conditions. Finkel *et al.* (1975) also considered that the charge separation of the fissure wall in the crystal material can produce an electrostatic field at an intensity of up to 10^9 V m^{-1}. Under such high electric field intensity, the gas or air between the coal fissures will be ionized and free electrons will be produced, thus providing a source of EMR generation. In addition, when the coal is broken, micro-fractures will cause deformation, dislocation, slip and so on, which can produce potential difference and make the electric field oscillate, and a large number of free electrons are excited thus undergoing irregular motions, forming varying electric and magnetic fields and thereby producing electromagnetic waves propagating outward.

Frid *et al.* (2003) hypothesized that electromagnetic waves are generated by charge oscillation on both sides of the propagating crack (see figure 16). Considering the line of bonds distributed in the tip of the propagating crack, when the crack expands forward to the next line nearby, the bonds between the two positions will be broken. After that, the atoms on both sides of the bonds are moved to the unbalanced positions, which relate to their steady-state positions and will oscillate around them. If each atom (ion) vibrates individually, the situation will be similar to the Einstein model of lattice vibration, and the frequency of these oscillations will be close to 10^{15} Hz. However, because the vibrational atomic lines move together and are also connected to the atoms around them (in the forward direction and also to atoms on their side of the two surfaces newly created by the fracture), the subsequent vibrations are similar to the obtained vibrations from the bulk by the Debye model that have much lower frequencies. It is this process that excites the oscillations on the new surfaces to produce EMR. More importantly, it can also be found that the Rayleigh wave velocity, v_R, in a material with a given Young's modulus E, Poisson ratio μ
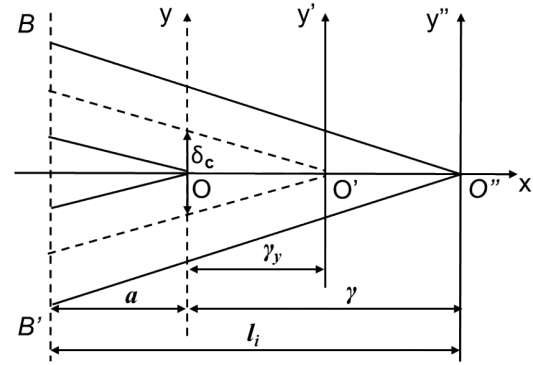
and density ρ, can be given by

$$v_R = \frac{0.87 + 1.12\mu}{1 + \mu} \sqrt{\frac{E}{2\rho(1 + \mu)}} \qquad (5)$$

Song *et al.* (2016) analyzed the typical characteristics of the electromagnetic signal from coal samples during the failure process due to uniaxial compression. Frequency changes in EMR from the loaded coal were investigated, and the relationship between the frequency of electromagnetic signals produced by crack expansion (shown in figure 17) and the physical parameters of coal was given by

$$f = \frac{1}{32\sqrt{\sqrt{2}l_i}} \frac{(0.87 + 1.12\mu)E^{\frac{3}{2}}}{(1 - \mu)(1 + \mu)^{\frac{5}{2}}\sigma_c\rho^{\frac{1}{2}}}, (l_i > a) \qquad (6)$$

where a is the initial crack length, l_i is defined as the crack length and equals the sum of the initial crack length and the extended length, i.e. $l_i = a + \gamma$. E is Young's modulus, μ is Poisson ratio, ρ is density and σ_c is yield strength and equals compressive strength in this case.

From equations (5) and (6), it can be seen that the micro-elastic modulus of coal is closely related to Rayleigh wave velocity and frequency of EMR. This study will be helpful to analyze the variation characteristics of electromagnetic signals from micro-fractures, which is of great significance for revealing the complexity and diversity of electromagnetic signals. Further analysis will be conducted in future research.

5. Conclusion

In this study, qualitative and quantitative analyses of heterogeneity of coal were performed according to the experimental results obtained by the optical microscope, digital micro-hardness tester and AFM. The electro-mechanical properties of coal were investigated at the micro- and nanoscale, and their effects on the EMR were discussed. Several conclusions are drawn:

(1) The optical microscope can clearly and qualitatively observe componential heterogeneity of coal samples at the microscale and this phenomenon is widespread. The qualitative test by the digital microhardness tester obtains the inhomogeneity of the mechanical properties of coal samples at the microscale.

(2) The electro-mechanical properties of coal samples were measured directly by AFM. The range of the micro-elastic modulus of XZY coal samples is 62.3 MPa–4.0 GPa, and the range of surface potential is 21.2–166.2 mV. The characteristics of the two show a normal distribution, which further illustrates the inhomogeneity of the electro-mechanical properties of coal samples at the micro- and nanoscale.

(3) The inhomogeneous elastic modulus causes the coal sample to break unevenly when loaded, and the surface potential difference in the dynamic failure process and the strong electric field intensity in the process can further excite the EMR due to the non-uniform migration of the charge.

Acknowledgements

Conflict of interest statement: The authors have no conflicts of interest to declare.

References

Adamcik, J., Lara, C., Usov, I., Jeong, J.S., Ruggeri, F.S., Dietler, G. & Mezzenga, R., 2012. Measurement of intrinsic properties of amyloid fibrils by the peak force QNM method, *Nanoscale*, **4**, 4426–4429.

Anderson, T.L., 2005. *Fracture Mechanics: Fundamentals and Applications.* Florida: CRC press.

Ashcroft, N.W. & Mermin, N.D., 1976. *Solid State Physics.* New York: Saunders College Publishing.

Bodzek, D. & Marzec, A., 1981. Molecular components of coal and coal structure, *Fuel*, **60**, 47–51.

Bruening, F.A. & Cohen, A.D., 2005. Measuring surface properties and oxidation of coal macerals using the Atomic Force Microscope, *International Journal of Coal Geology*, **63**, 195–204.

Butt, H.J., Cappella, B. & Kappl, M., 2005. Force measurements with the atomic force microscope: technique, interpretation and applications, *Surface Science Reports*, **59**, 1–152.

Christopher, A.J., Zachary, C.G. & James, A.O., 2012. Measurement of elastic properties of calcium silicate hydrate with atomic force microscopy, *Cement & Concrete Composites*, **34**, 468–477.

Clark, N., Oikonomou, A. & Vijayaraghavan, A., 2013. Ultrafast quantitative nanomechanical mapping of suspended graphene, *Physica Status Solidi B – Basic Solid State Physics*, **250**, 2672–2677.

Collins, L., Tselev, A., Jesse, S., Okatan, M.B., Proksch, R., Mathews, J.P. & Ivanov, I.N., 2014. Breaking the limits of structural and mechanical imaging of the heterogeneous structure of coal macerals, *Nanotechnology*, **25**, 417–435.

Dokukin, M.E. & Sokolov, I., 2012. Quantitative mapping of the elastic modulus of soft materials with Harmoni X and Peak Force QNM AFM modes, *Langmuir*, **28**, 16060–16071.

Dou, L.M., Tian, J.C., Lu, C.P., Wu, X.R., Mou, Z.L., Zhang, X.T. & Li, Z.H., 2005. Research on electromagnetic radiation rules of composed coal-rock burst failure. *Chinese Journal of Rock Mechanics and Engineering*, **24**, 3541–3544.

Du, Y., Zhang, Y., Zhang, C. & Liu, Y., 2015. In situ nanoindentation mechanical property of films by atomic force microscope, *Rare Metal Materials and Engineering*, **44**, 1959–1963.

Enomoto, Y., Akai, M., Hashimoto, H., Mori, S. & Asabe, Y., 1993. Exo-electron emission: Possible relation to seismic geo-electromagnetic activities as a microscopic aspect in geotribology, *Wear*, **168**, 135–142.

Fernández, R., Ocando, C., Fernandes, S.C., Eceiza, A. & Tercjak, A., 2014. Optically active multilayer films based on chitosan and an azopolymer, *Biomacromolecules*, **15**, 1399–1407.

Frankel, V.M., Golovin, Y.I. & Serea, V.Z., 1975. Electrical effects accompanying fracture of LIF crystals and problem of crack control. *Soviet Physics – Solid State*, **17**, 492–495.

Frid, V., 1997. Electromagnetic radiation method for rock and gas outburst forecast. *Journal of Applied Geophysics*, **38**, 97–104.

Frid, V, Rabinovitch, A. & Bahat, D., 2003. Fracture induced electromagnetic radiation, *Journal of Physics D: Applied Physics*, **36**, 1620–1628.

Frid, V. & Vozoff, K., 2005. Electromagnetic radiation induced by mining rock failure. *International Journal of Coal Geology*, **64**, 57–65.

Gade, S., Alaca, B. & Sause, M., 2017. Determination of crack surface orientation in carbon fibre reinforced polymers by measuring electromagnetic emission, *Journal of Nondestructive Evaluation*, **36**, 21.

Gao, Z., Hu, Y., Sun, W. & Drelich, J.W., 2016. Surface-charge anisotropy of scheelite crystals, *Langmuir*, **32**, 6282–6288.

Garner-O'Neale, L.D., Bonamy, A.F., Meek, T.L. & Patrick, B.G., 2003. Calculating group electronegativities using the revised Lewis–Langmuir equation. *Journal of Molecular Structure: Theochem*, **639**, 151–156.

Guo, Y. & Yu, X., 2017. Characterizing the surface charge of clay minerals with Atomic Force Microscope (AFM), *AIMS Materials Science*, **4**, 582–593.

Guo, Z. & Liu, B. 1995. Frequency properties of electromagnetic emission associated with microscopic cracking in rocks, *Chinese Journal of Geophysics – Chinese Edition*, **4**, 59.

He, M., Li, Z., Liu, J. & Liu, Y., 2013. Experimental study on surface current of coal under uniaxial compression, *Journal of China Coal Society*, **38**, 966–969.

He, X., Chen, W., Nie, B. & Zhang, M., 2010. Classification technique for danger classes of coal and gas outburst in deep coal mines, *Safety Science*, **48**, 173–178.

He, X., Liu, X., Nie, B. & Song, D., 2017. FTIR and Raman spectroscopy characterization of functional groups in various rank coals, *Fuel*, **206**, 555–563.

He, X., Liu, X., Song, D. & Nie, B., 2019. Effect of microstructure on electrical property of coal surface. *Applied Surface Science*, **483**, 713–720.

He, X., Nie, B., Chen, W., Wang, E., Dou, L., Wang, Y., Liu, M. & Mitri, H., 2012. Research progress on electromagnetic radiation in gas-containing coal and rock fracture and its applications, *Safety Science*, **50**, 728–735.

He, X., Wang, E., Nie, B., Liu, M. & Zhang, L., 2003. *Rheological Electromagnetic Dynamics of Coal and Rock*. Beijing: Science Press.

Huang, L., Fang, H. & Chen, M., 2012a. Experiment on surface charge distribution of fine sediment, *Science China – Technological Sciences*, **55**, 1146–1152.

Huang, L., Fang, H., Chen, M. & Zhao, H., 2012b. Review of surface charge characteristics of fine sediment, *Journal of Tsinghua University (Science and Technology)*, **52**, 747–751.

Kumar, N., Zhao, C., Klaassen, A., van den Ende, D., Mugele, F. & Siretanu, I., 2016. Characterization of the surface charge distribution on kaolinite particles using high resolution atomic force microscopy, *Geochimica ET Cosmochimica Acta*, **175**, 100–112.

Li, T. & Zeng, K., 2014, Nanoscale elasticity mappings of micro-constituents of abalone shell by band excitation-contact resonance force microscopy, *Nanoscale*, **6**, 2177–2185.

Li, Z., Lou, Q., Wang, E., Liu, S. & Niu, Y., 2017. Study on acoustic–electric–heat effect of coal and rock failure processes under uniaxial compression. *Journal of Geophysics and Engineering*, **15**, 71–80.

Li, Z., Wang, E. & He, X., 2012. *Study on Theory and Mechanism of Surface Potential Effect of Coal and Rock Failure.* Xuzhou: China University of Mining and Technology Press.

Li, Z., Wang, E., Liu, Z., Song, X. & Li, Y., 2009. Study on characteristics and rules of surface potential during coal fracture, *Journal of China University of Mining & Technology*, **38**, 187–192.

Liscio, A., Palermo, V., Mullen, K. & Samori, P., 2008. Tip-sample interactions in Kelvin probe force microscopy: quantitative measurement of the local surface potential, *Journal of Physical Chemistry C*, **112**, 17368–17377.

Liu, J., Wang, J., Huang, J., Cui, X., Tan, X., Liu, Q. & Zeng, H., 2017. Heterogeneous distribution of adsorbed bitumen on fine solids from solvent-based extraction of oil sands probed by AFM, *Energy & Fuels*, **31**, 8833–8842.

Liu, X. & Nie, B., 2016. Fractal characteristics of coal samples utilizing image analysis and gas adsorption. *Fuel*, **182**, 314–322.

Liu, X., Song, D., He, X., Nie, B. & Wang, L., 2019. Insight into the macromolecular structural differences between hard coal and deformed soft coal. *Fuel*, **245**, 188–197.

Lv, X., Pan, Y., Xiao, X. & Wang, A., 2013. Barrier formation of micro-crack interface and piezoelectric effect in coal and rock masses, *International Journal of Rock Mechanics & Mining Sciences*, **64**, 1–5.

Mastrogiannis, D., Antsygina, T.N., Chishko, K.A., Mavromatou, C. & Hadjicontis, V., 2015. Relationship between electromagnetic and acoustic emissions in deformed piezoelectric media: microcracking signals. *International Journal of Solids and Structures*, **56**, 118–125.

Miura, K., Mae, K., Shimada, M. & Minami, H., 2001. Analysis of formation rates of sulfur-containing gases during the pyrolysis of various coals, *Energy & Fuels*, **15**, 629–636.

Nie, B., Liu, X., Yang, L., Meng, J. & Li, X., 2015. Pore structure characterization of different rank coals using gas adsorption and scanning electron microscopy, *Fuel*, **158**, 908–917.

Nitsan, U., 1977. Electromagnetic emission accompanying fracture of quartz-bearing rocks, *Geophysical Research Letters*, **4**, 333–336.

Ogawa, T., Oike, K. & Miura, T., 1985. Electromagnetic radiations from rocks, *Journal of Geophysical Research – Atmospheres*, **90**, 6245–6249.

O'Keefe, S.G. & Thiel, D.V., 1995. A mechanism for the production of electromagnetic radiation during fracture of brittle materials, *Physics of the Earth and Planetary Interiors*, **89**, 127–135.

Park, S.K., Johnston, M.J., Madden, T.R., Morgan, F.D. & Morrison, H.F., 1993. Electromagnetic precursors to earthquakes in the ULF band: a review of observations and mechanisms, *Reviews of Geophysics*, **31**, 117–132.

Potgieter-Vermaak, S., Maledi, N., Wanger, N., Van Heerden, J.H.P., Van Grieken, R. & Potgieter, J.H., 2011. Raman spectroscopy for the analysis of coal: a review, *Journal of Raman Spectroscopy*, **42**, 123–129.

Qiu, L., Li, Z., Wang, E., Liu, Z., Ou, J., Li, X., Ali, M., Zhang, Y. & Xia, S., 2018. Characteristics and precursor information of electromagnetic signals of mining-induced coal and gas outburst. *Journal of Loss Prevention in the Process Industries*, **54**, 206–215.

Qiu, L., Wang, E., Song, D., Liu, Z., Shen, R., Lv, G. & Xu, Z., 2017. Measurement of stress field of tunnel through its rock EMR, *Journal of Geophysics and Engineering*, **14**, 949–959.

Rabinovitch, A., Frid, V. & Bahat, D., 1998. Parametrization of electromagnetic radiation pulses obtained by triaxial fracture of granite sample, *Philosophical Magazine Letters*, **77**, 289–293.

Rabinovitch, A., Frid, V. & Bahat, D., 2007, Surface oscillations – a possible source of fracture induced electromagnetic radiation, *Tectonophysics*, **413**, 15–21.

Solum, M.S., Pugmire, R.J., Grant, D.M., Kelemen, S.R., Gorbaty, M.L. & Wind, R.A., 1997. ^{15}N CPMAS NMR of the Argonne premium coals, *Energy & Fuels*, **11**, 491–494–959.

Song, X., Li, X., Li, Z., Zhang, Z., Cheng, F., Chen, P. & Liu, Y., 2018. Study on the characteristics of coal rock electromagnetic radiation (EMR) and the main influencing factors. *Journal of Applied Geophysics*, **148**, 216–225.

Song, D., Wang, E., Li, Z., Qiu, L. & Xu, Z. 2017. EMR: an effective method for monitoring and warning of rock burst hazard. *Geomechanics and Engineering*, **12**, 53–69.

Song, D., Wang, E., Song, X., Jin, P. & Qiu, L., 2016. Changes in frequency of electromagnetic radiation from loaded coal rock, *Rock Mechanics and Rock Engineering*, **49**, 291–302.

Trtik, P., Kaufmann, J. & Volz, U., 2012. On the use of peak-force tapping atomic force microscopy for quantification of the local elastic modulus in hardened cement paste, *Cement and Concrete Research*, **42**, 215–221.

Tsukruk, V.V., Shulha, H. & Zhai, X., 2003. Nanoscale stiffness of individual dendritic molecules and their aggregates, *Applied Physics Letters*, **82**, 907–909.

Wang, C., Xu, J., Zhao, X. & Wei, M., 2012. Fractal characteristics and its application in electromagnetic radiation signals during fracturing of coal or rock. *International Journal of Mining Science and Technology*, **22**, 255–258.

Wang, D., Liang, X., Russell, T.P. & Nakajima, K., 2014. Visualization and quantification of the chemical and physical properties at a diffusion-induced interface using AFM nanomechanical mapping, *Macromolecules*, **47**, 3761–3765.

Wang, E. & He, X., 2000. An experiment study of the electromagnetic emission during the deformation and fracture of coal or rock, *Chinese Journal of Geophysics – Chinese Edition*, **43**, 131–140.

Wang, E., He, X., Li, Z. & Zhao, E., 2009. *Technology and Application of Coal and Rock Electromagnetic Radiation*, Science Press, Beijing.

Yan, L., Englert, A.H., Masliyah, J.H. & Xu, Z., 2011. Determination of anisotropic surface characteristics of different phyllosilicates by direct force measurements, *Langmuir*, **27**, 12996–13007.

Yao, S., Jiao, K., Zhang, K., Hu, W., Ding, H., Li, M. & Pei, W., 2011. An atomic force microscopy study of coal nanopore structure, *Chinese Science Bulletin*, **56**, 1820–1827.

Yin, X. & Drelich, J., 2008. Surface charge microscopy: novel technique for mapping charge-mosaic surfaces in electrolyte solutions, *Langmuir*, **24**, 8013–8020.

Young, T.J., Monclus, M.A., Burnett, T.L., Broughton, W.R., Ogin, S.L. & Smith, P.A., 2011. The use of the Peak Force (TM) quantitative nanomechanical mapping AFM-based method for high-resolution Young's modulus measurement of polymers, *Measurement Science and Technology*, **22**, 125703.

Yu, S. & Feng, X., 1997. *Damage Mechanics.* Tsinghua University Press, Beijing.